JCTC Journal of Chemical Theory and Computation

ARTICLE

pubs.acs.org/JCTC

Scalar Relativistic Computations of Nuclear Magnetic Shielding and *g*-Shifts with the Zeroth-Order Regular Approximation and Range-Separated Hybrid Density Functionals

Fredy Aquino,[†] Niranjan Govind,[‡] and Jochen Autschbach*,[†]

[†]Department of Chemistry, State University of New York at Buffalo, Buffalo, New York 14260-3000

[‡]William R. Wiley Environmental Molecular Sciences Laboratory, Pacific Northwest National Laboratory, 902 Battelle Blvd, P.O. Box 999, Mail Stop K8-91 Richland, Washington 99352, United States

Supporting Information

ABSTRACT: Density functional theory (DFT) calculations of NMR chemical shifts and molecular *g* tensors with Gaussian-type orbitals are implemented via second-order energy derivatives within the scalar relativistic zeroth order regular approximation (ZORA) framework. Nonhybrid functionals, standard (global) hybrids, and range-separated (Coulomb-attenuated, long-range corrected) hybrid functionals are tested. Origin invariance of the results is ensured by use of gauge-including atomic orbital (GIAO) basis functions. The new implementation in the NWChem quantum chemistry package is verified by calculations of nuclear shielding constants for the heavy atoms in HX (X = F, Cl, Br, I, At) and H_2X (X = O, S, Se, Te, Po) and ^{125}Te chemical shifts in a number of tellurium compounds. The basis set and functional dependence of *g*-shifts is investigated for 14 radicals with light and heavy atoms. The problem of accurately predicting ^{19}F NMR shielding in $UF_{6-n}Cl_n$, $n = 1-6$, is revisited. The results are sensitive to approximations in the density functionals, indicating a delicate balance of DFT self-interaction vs correlation. For the uranium halides, the range-separated functionals are not clearly superior to global hybrids.

1. INTRODUCTION

Magnetic resonance spectroscopy is of high importance in basic and applied research. In the past decades, much effort has been directed at computations of such parameters for molecules starting from first principles theory.[1−7] This report is concerned with NMR nuclear magnetic shielding as well as electron paramagnetic resonance (EPR) *g*-shifts and, more specifically, with relativistic effects. A free electron has a *g* factor of $g_e \approx 2.0023$. A deviation of *g* from g_e, associated with the effective spin of a molecule, is linked to spin−orbit (SO) coupling, which is a relativistic effect. The *g* shift tensor Δg quantifies the deviation from the isotropic free electron case and represents one of the sets of parameters that defines the EPR spectrum.[8] The *g* tensor is also important when considering paramagnetic effects in the NMR of open shell molecules.[9−12] The "regular" NMR shielding has a nonvanishing, nonrelativistic limit. However, due to the nature of the quantum mechanical operators involved in its calculation, relativistic effects on NMR shieldings can be highly significant and have been the subject of much theoretical work spanning several decades.[2,13−19]

The method of choice for first-principles computations of magnetic resonance parameters of large molecules with heavy elements and metal complexes is density functional theory (DFT), due to its attractive balance of computational cost and the accuracy level that can be attained in the computations. The combination of DFT with the approximate two-component relativistic zeroth-order regular approximation (ZORA)[20,21] represents an efficient way of carrying out correlated relativistic electronic structure calculations. ZORA is one among several efficient methods available to perform relativistic electronic structure and magnetic property calculations. Among the more widely applied methods, we mention the two-component Douglas−Kroll−Hess approach[22−24] and (usually somewhat more demanding) fully relativistic methods.[25] The ZORA Hamiltonian has been found to be a suitable choice for computations of magnetic resonance parameters[26−35] because it can accurately generate relativistic effects for molecular properties that are dominated by valence orbital contributions, such as NMR chemical shifts, *J*-coupling, and *g*-shifts. Further, it is straightforward to derive ZORA perturbation operators for magnetic properties, and to calculate matrix elements thereof, using numerical integration. In molecular DFT calculations where numerical integration of the exchange-correlation (XC) potential and the associated response kernels is standard practice, one might argue that there is not much to gain from calculating ZORA perturbation operator matrices fully analytically because such techniques require additional approximations.[36] We note, however, that analytic integrals can be utilized in ZORA computations, for instance by separating nonrelativistic contributions from integrals involving relativistic operators.[37] Magnetic resonance calculations reported in the works cited above have utilized the ZORA implementations of the Amsterdam Density Functional (ADF) package.[38] This code employs Slater-type orbital (STO) basis sets and density fitting for calculating the Coulomb potential and has already for a long time incorporated methods for ZORA calculations of a variety of NMR and EPR parameters as well as other molecular response properties. Hybrid DFT functionality

Received: June 15, 2011
Published: September 14, 2011

for magnetic resonance parameters in this STO-based program has been reported recently.[28,31,35,39]

Herein, we report the development of a ZORA methodology for scalar relativistic DFT computations for NMR shielding tensors and EPR Δg tensors in the NWChem package,[37] utilizing gauge-including atomic orbitals (GIAOs) to ensure origin-invariant results. The implementation makes use of the coupled-perturbed Hartree−Fock equation solver originating in Dupuis' nonrelativistic GIAO shielding implementation in NWChem,[40] which would have to be redesigned to enable spin−orbit calculations. NWChem employs Gaussian-type orbital (GTO) basis sets for molecular calculations. Its DFT module has recently been extended[41−46] to allow for computations with range-separated hybrid functionals.[47−49] This class of functionals shows promise for alleviating certain problems in DFT and time-dependent DFT calculations of response properties such as the correct asymptotic behavior of the potential and the treatment of charge transfer. The ZORA implementation for NMR and EPR utilizes numerical integration methods for operator matrix elements that we recently implemented in NWChem for relativistic calculations of electric field gradients.[50] The availability of the new static linear response ZORA functionality developed for this work is used to investigate the performance of relativistic magnetic resonance DFT calculations in conjunction with range-separated hybrid functionals. Further, we aim to test the suitability of relatively common Gaussian-type basis sets (such as the ones used in previous work on ZORA electric field gradients) for scalar ZORA NMR chemical shift and EPR g shift computations.

There is a body of data showing that nonhybrid functionals occasionally perform poorly in calculations of g-shifts ranging from light organic radicals to heavy metal complexes[10,24,51−58] and NMR shielding in metal complexes.[13,19,59−61] Standard (global) hybrid functionals also do not consistently perform well, in particular for metal complexes. It is therefore interesting to investigate the performance of range-separated hybrids in conjunction with a relativistic method. As an example, fluorine chemical shifts in U(VI) complexes have been determined previously with nonrelativistic hybrid DFT computations employing a relativistic ECP for uranium.[60,62] It was found that the ^{19}F chemical shifts are sensitive to the computational model. For instance, the ordering of the fluorine shift in UF_6 versus *fac*-UF_3Cl_3 is predicted incorrectly with nonhybrid functionals and the B3LYP hybrid functional, whereas the correct ordering is obtained with the BHLYP functional, which has a much larger fraction of Hartree−Fock (HF) exchange than B3LYP (50 vs 20%). In a benchmark study of molecular g-tensors, we determined recently that the PBE0 hybrid performed similarly to the nonhybrid PBE functional across a small-molecule test set including inorganic and organic radicals with light and heavy metal atoms,[35] but it is unclear yet how all-electron relativistic calculations with range-separated hybrid functionals perform in comparison. For the case of the ^{19}F shielding in $UF_{6-n}Cl_n$, n = 1−6, it is shown herein that there is a difficult balance between reproducing the magnitude of the shielding and trends such as UF_6 versus *fac*-UF_3Cl_3 where hybrid functionals with a large fraction of HF exchange perform better, and other trends among the set of complexes that appear to be better reproduced with nonhybrid functionals and B3LYP, albeit with an overall too small magnitude of the ^{19}F shieldings. The range-separated hybrids yield shielding constants that are closer to experimental results and to calculations with 50% global hybrids, without achieving a breakthrough improvement over the latter. For the g shift test set, we find comparable results calculated with CAM-B3LYP and the PBE0 global hybrid (25% HF exchange).

Following this Introduction, theoretical details of the ZORA linear response shielding and g shift calculations are provided in section 2 along with details about the implementation, such as the numerical integration of the relevant perturbation operator matrix elements. Computational details are provided in section 3. Results from various benchmark computations are provided in section 4 in order to verify the implementations and investigate the performance of nonhybrid vs hybrid DFT with global fixed fractions of HF exchange vs range-separated hybrid functionals. This work concludes with a brief summary and outlook in section 5.

2. THEORETICAL METHODS

A component of the chemical shift tensor can be calculated within a DFT framework from variational perturbation theory as a second derivative of the energy E as

$$\sigma_{uv} = \frac{\partial^2 E}{\partial B_u \partial \mu_v} \tag{1}$$

Here, B_u is the component of an external magnetic field, and μ_v is a component of the nuclear spin magnetic moment vector of the nucleus at which the shielding tensor is calculated, and $u,v \in \{x,y,z\}$. Here and elsewhere, it is assumed that magnetic-field-related perturbation parameter derivatives are taken at $B_u = 0$ and $\mu_v = 0$. Within a scalar relativistic or nonrelativistic framework, one can also define the components of the electronic g-tensor as a second derivative of the molecular energy[63]

$$g_{uv} = \frac{1}{\beta_e}\frac{\partial^2 E}{\partial B_u \partial S_v} \tag{2}$$

in which case spin−orbit coupling is treated as a perturbation and not included in the ground state calculation. Here, S_v is a component of the effective spin vector of the molecule. The Bohr magneton $\beta_e = e\hbar/(2m_e)$ enters the expression based on usual conventions for the EPR spin Hamiltonian.[8] In the Dirac theory of the electron, the free electron g_e is exactly 2. In the following, atomic units where $g_e\beta_e = 1$ are used. The calculations determine g-shifts Δg directly as deviations from the free electron g value. Therefore, it is not necessary to specify a particular value for g_e in the implementation.

As Schreckenbach and Ziegler have demonstrated within the framework of the Pauli Hamiltonian,[63] the computational machineries for shielding and Δg tensors based on eqs 1 and 2 share many common components. Functionality for shielding and Δg tensors can therefore be developed in a concerted fashion. The calculations for Δg and NMR shielding reported here include scalar relativistic effects variationally in E. For g-shifts, spin−orbit (SO) coupling is treated as a perturbation. For shielding tensors, the effects from SO coupling are presently neglected. Some research groups have developed theoretical methods for calculations of g tensors as *first* derivatives of the energy instead, with SO coupling included variationally in the unperturbed set of orbitals,[34,55−57,64] We plan to investigate such an approach in conjunction with ZORA in a follow-up report. A recent comparison of the first-order and second-order derivative methods in their respective implementations in the ADF code using ZORA in conjunction with STO basis sets has shown that they can yield comparable results[35] overall, with the notable exception of the

known symmetry-related breakdown of the second-order approach for the Δg tensor components in linear molecules.[65] In this context, we note recent work by Hrobarik et al. where differences in treating SO coupling as a first-order perturbation versus as a higher order one were found to be significant.[66]

For the shielding tensor calculations, a closed-shell reference is assumed. The *g*-tensor calculations are based on spin-unrestricted DFT computations. In a scalar relativistic spin-unrestricted Kohn−Sham DFT approach with singly occupied pure α and β spin orbitals, the maximum spin projection is

$$S_z = \frac{n_\alpha - n_\beta}{2} \tag{3}$$

where n_α and n_β are the numbers of occupied orbitals of α and β spins, respectively. The "spin derivative" in eq 2 as well as the associated operator derivatives (vide infra) are understood to be taken in the expectation value after the action of spin dependent operators on the orbitals has been considered. This procedure leads to an overall factor of S_z^{-1} in the final expression for the *g*-tensor and to contributions of opposite signs from α and β spin orbitals, respectively. For details and a review of pertinent literature see refs 5, 6, and 35 as well as the review articles by Kaupp et al. and Neese cited in the Introduction. In the NMR shielding tensor calculations, the contributions from α and β orbitals reinforce each other.

The ZORA one-electron Fock operator used in DFT with a local effective potential *V* reads in atomic units:[20]

$$\begin{aligned}\hat{h} &= V + \frac{1}{2}(\vec{\sigma}\cdot\hat{\boldsymbol{p}})\mathscr{K}(\vec{\sigma}\cdot\hat{\boldsymbol{p}}) \\ &= V + \frac{1}{2}\hat{\boldsymbol{p}}\cdot\mathscr{K}\hat{\boldsymbol{p}} + \frac{1}{2}i\vec{\sigma}\cdot(\hat{\boldsymbol{p}}\mathscr{K}\times\hat{\boldsymbol{p}})\end{aligned} \tag{4}$$

with

$$\mathscr{K} = \frac{2c^2}{2c^2 - V} \tag{5}$$

Further, $\vec{\sigma}$ is the 3-vector of 2 × 2 Pauli spin matrices, with components $\vec{\sigma} = (\sigma_x\sigma_y\sigma_z)$, and $\hat{\boldsymbol{p}} = -i\nabla$ is the momentum operator. The last term in eq 4 is the ZORA spin−orbit operator which, for the purpose of this work, is neglected in the shielding computations and included as a perturbation in the *g* shift calculations. The unperturbed Kohn−Sham orbitals $\varphi_i^{(0)}$ are determined with the scalar relativistic ZORA (ZORA-SR) Fock operator

$$\hat{h}^{(0)} = V + \frac{1}{2}\hat{\boldsymbol{p}}\cdot\mathscr{K}\hat{\boldsymbol{p}} \tag{6}$$

The potential *V* in eqs 4 and 6 is determined self-consistently for systems with more than one (spin) orbital and may be adapted in the usual way for standard and range-separated hybrid functionals to include exact exchange contributions. The potential *V* used to construct $\mathscr{K}$ in eq 5 is in the NWChem implementation approximated as a sum of (local) atomic Hartree potentials V_A as $V \approx \Sigma_A V_A$.[37,50] A related approach was taken by van Wüllen for a ZORA implementation in the Turbomole code[67] and by Philipsen et al. for an implementation in the Amsterdam Density functional (ADF) package.[68] Such approximations in the ZORA operator have since been demonstrated to be a practical and accurate way to enable ZORA relativistic computations for large systems.

The shielding and the *g*-tensor involve magnetic field derivatives. In order to avoid origin-dependent results, we adopt a "gauge-including atomic orbital" (GIAO)[69,70] basis set. In terms of a standard atom-centered GTO or STO basis set $\{\chi_s\}$, the GIAOs $\xi_s(\boldsymbol{B})$ are given as

$$\xi_s(B) = \chi_s \exp\left[-\frac{i}{2}(\boldsymbol{B}\times\boldsymbol{R}_s)\cdot\boldsymbol{r}\right] \tag{7}$$

where $\boldsymbol{R}_s$ is the center of the AO basis function χ_s. Below, the electron location with respect to a basis function center, $\boldsymbol{r}_s = \boldsymbol{r} - \boldsymbol{R}_s$, is used frequently. The coefficients for the unperturbed MOs in the basis set are denoted as $C_{si}^{(0)}$. The basis set coefficients of the magnetic field perturbed MOs for field direction *u* are $C_{ri}^{(u)}$. It is beneficial to utilize elements of the scalar relativistic density (+) and spin-density (−) matrices in the AO basis given by

$$P_{rs}^{(0)\alpha\pm\beta} = \sum_i n_i^\alpha\, C_{ri}^{(0)\alpha} C_{si}^{*(0)\alpha} \pm \sum_i n_i^\beta\, C_{ri}^{(0)\beta} C_{si}^{*(0)\beta} \tag{8a}$$

and

$$\begin{aligned}P_{rs}^{(u)\alpha\pm\beta} = &\sum_i n_i^\alpha [C_{ri}^{(0)\alpha} C_{si}^{*(u)\alpha} + C_{ri}^{(u)\alpha} C_{si}^{*(0)\alpha}] \\ &\pm \sum_i n_i^\beta [C_{ri}^{(0)\beta} C_{si}^{*(u)\beta} + C_{ri}^{(u)\beta} C_{si}^{*(0)\beta}]\end{aligned} \tag{8b}$$

where the n_i^γ, γ = α and β, are the occupation numbers for the spin orbitals. For the magnetic field perturbation and real one-component unperturbed orbitals, the perturbed orbital and spin-density matrices are imaginary. For the calculation of the perturbed MO coefficients, we employ a modified version of the coupled-perturbed Kohn−Sham (CPKS) equation solver that was originally implemented in NWChem by Dupuis[40] for the purpose of nonrelativistic NMR calculations. The ZORA functionality incorporates extensions for the computation of DFT contributions to the perturbed Fock matrices used to determine the $C_{ri}^{(u)}$. These modifications entail the use of numerical integration to determine AO matrix elements for a scalar ZORA external magnetic field perturbation operator suitable for GIAO computations:

$$\hat{h}_{rs}^{(u)} = -\frac{i}{4}[\mathscr{K}(\boldsymbol{r}_r\times\nabla)_u + (\boldsymbol{r}_s\times\nabla)_u\mathscr{K}] \tag{9}$$

and the use of the unperturbed ZORA Fock operator, eq 6, in GIAO magnetic field derivatives of the Fock operator matrix elements needed in the CPKS solver,[40] which requires matrix elements of

$$\hat{h}_{rs}^{\mathrm{SR},(u)} = -\frac{i}{4}\nabla\mathscr{K}[\boldsymbol{r}\times(\boldsymbol{R}_s - \boldsymbol{R}_r)]_u\cdot\nabla \tag{10}$$

Another modification has been necessary in the CPKS solver related to the calculation of two-electron integrals and their GIAO magnetic field derivatives, which are calculated in NWChem using Rys quadrature. These modifications are described in the Appendix. For further details regarding the CPKS procedure, we refer the reader to Dupuis' original paper,[40] which expands on many of the associated technical details.

Working expressions that were implemented for the calculation of GIAO chemical shift and Δg tensor elements are as follows:

Diamagnetic nuclear magnetic shielding, nucleus Q:

$$\sigma^{d}_{uv} = \sum_{r,s} P^{(0)\alpha+\beta}_{rs}\left[\langle\chi_r|\frac{1}{2}[\hat{h}^{(u,v)}_{r,Q} + \hat{h}^{(u,v)}_{s,Q}]|\chi_s\rangle + \langle\chi_r|\hat{R}^{(u,v)}_{rs,Q}|\chi_s\rangle\right] \tag{11a}$$

Paramagnetic nuclear magnetic shielding, nucleus Q:

$$\sigma^{p}_{uv} = \sum_{r,s}\left[2Re\left\{P^{(u)\alpha+\beta}_{rs}\langle\chi_r|\hat{h}^{(v)}_{Q}|\chi_s\rangle\right\} + P^{(0)\alpha+\beta}_{rs}\frac{i}{2}(\boldsymbol{R}_r\times\boldsymbol{R}_s)_u\langle\chi_r|\hat{h}^{(v)}_{Q}|\chi_s\rangle\right] \tag{11b}$$

Diamagnetic Δg:

$$\Delta g^{d}_{uv} = \frac{4}{n_\alpha - n_\beta}\sum_{r,s} P^{(0)\alpha-\beta}_{rs}[\langle\chi_r|\hat{h}^{(u,v)}_{s}|\chi_s\rangle + \langle\chi_r|\hat{R}^{(u,v)}_{rs}|\chi_s\rangle] \tag{12a}$$

Paramagnetic Δg:

$$\Delta g^{p}_{uv} = \frac{4}{n_\alpha - n_\beta}\sum_{r,s}\left[2Re\left\{P^{(u)\alpha-\beta}_{rs}\langle\chi_r|\hat{h}^{(v)}|\chi_s\rangle\right\} + P^{(0)\alpha-\beta}_{rs}\frac{i}{2}(\boldsymbol{R}_r\times\boldsymbol{R}_s)_u\langle\chi_r|\hat{h}^{(v)}|\chi_s\rangle\right] \tag{12b}$$

The prefactors in eq 12 represent $1/(\beta_e S_z)$, where eq 3 has been used for the effective spin. Going back to a suggestion by Fukui,[71] GIAO-related terms have been grouped to yield diamagnetic and paramagnetic shielding and Δg tensors that are individually origin-independent. The total tensors are given by the sum of the paramagnetic and diamagnetic components. The various operators in eqs 11 and 12 are as follows:

Shielding tensor, eq 11:

$$\hat{h}^{(v)}_{Q} = -\frac{i}{2}[\mathscr{K}\frac{(\boldsymbol{r}_Q\times\nabla)_v}{r^3_Q} + \frac{(\boldsymbol{r}_Q\times\nabla)_v}{r^3_Q}\mathscr{K}] \tag{13a}$$

$$\hat{h}^{(u,v)}_{s,Q} = \frac{\mathscr{K}}{2r^3_Q}(\delta_{uv}\boldsymbol{r}_Q\cdot\boldsymbol{r}_s - r_{Q,u}r_{s,v}) \tag{13b}$$

$$\hat{R}^{(u,v)}_{rs,Q} = \frac{1}{4}[\frac{(\boldsymbol{r}_Q\times\nabla)_v}{r^3_Q}\mathscr{K}[\boldsymbol{r}_r\times(\boldsymbol{R}_s-\boldsymbol{R}_r)]_u + \tag{13c}$$

$$\mathscr{K}[\boldsymbol{r}_s\times(\boldsymbol{R}_s-\boldsymbol{R}_r)]_u\frac{(\boldsymbol{r}_Q\times\nabla)_v}{r^3_Q}] \tag{13d}$$

Δg tensor, eq 12:

$$\hat{h}^{(v)} = -\frac{i}{2}(\nabla\mathscr{K}\times\nabla)_v \tag{13e}$$

$$\hat{h}^{(u,v)}_{s} = \frac{1}{4}\{\delta_{uv}\nabla\cdot(\mathscr{K}-1)\boldsymbol{r}_s - \nabla_u(\mathscr{K}-1)r_{s,v}\} \tag{13f}$$

$$\hat{R}^{(u,v)}_{rs} = \frac{i}{2}[\boldsymbol{r}_s\times(\boldsymbol{R}_s-\boldsymbol{R}_r)]_u\hat{h}^{(v)} \tag{13g}$$

Curly brackets indicate where derivatives are taken only in the operator, i.e., where ∇ is not acting on any basis functions or orbitals to the right. Using $(\mathscr{K}-1)$ instead of $\mathscr{K}$ in eq 13f has the effect of subtracting the free electron g value from the calculated g-tensor, and thus eq 12 yields Δg. Magnetic perturbation operators in ZORA typically afford derivatives of $\mathscr{K}$. AO matrix elements of the operators are calculated in our implementation by numerical integration. By using the turnover rule for the momentum operator and/or partial integration, derivatives of $\mathscr{K}$ can be switched over to the basis functions χ_r and χ_s instead.

Matrix elements for the external magnetic field operator, eq 9, are calculated as

$$H^{(u)}_{rs} = \frac{i}{4}(L_{rs,mn} - L^{*}_{sr,mn} - [L_{rs,nm} - L^{*}_{sr,nm}]) \tag{14a}$$

with $L_{rs,mn}$ given in terms of basic AO integrals as

$$L_{rs,mn} = \langle\frac{\partial\chi_r}{\partial r_n}|\mathscr{K}r_m|\chi_s\rangle - R_{s,m}\langle\frac{\partial\chi_r}{\partial r_n}|\mathscr{K}|\chi_s\rangle \tag{14b}$$

where $umn = xyz,yzx,zxy$. Matrix elements for the scalar relativistic operator of eq 10 were implemented as

$$H^{\mathrm{SR},(u)}_{rs} = \frac{i}{4}[R_{sr,b}\sum_p Y_{rs,pp,a} - R_{sr,a}\sum_p Y_{rs,pp,b}] \tag{14c}$$

with $\boldsymbol{R}_{sr} = \boldsymbol{R}_s - \boldsymbol{R}_r$, $uab = xyz,yzx,zxy$, and basic AO integrals $Y_{rs,pq,a}$ given as

$$Y_{rs,pq,a} = \langle\frac{\partial\chi_r}{\partial r_p}|r_a\mathscr{K}|\frac{\partial\chi_s}{\partial r_q}\rangle \tag{14d}$$

Matrix elements of the ZORA analog of the paramagnetic spin−orbital (PSO) operator, eq 13a, were implemented as

$$H^{(v)}_{rs,Q} = \frac{i}{2}(N_{rs,mn} - N^{*}_{sr,mn} - [N_{rs,nm} - N^{*}_{sr,nm}]) \tag{14e}$$

with $N_{rs,mn}$ given as

$$N_{rs,mn} = \langle\frac{\partial\chi_r}{\partial r_n}|\mathscr{K}\frac{r_{Q,m}}{r^3_Q}|\chi_s\rangle \tag{14f}$$

where $vmn = xyz,yzx,zxy$.

Matrix elements of the ZORA diamagnetic GIAO shielding operator eq 13b, were implemented as

$$H^{(u,v)}_{rs,Q} = \frac{1}{4}\begin{cases} -I^{(u,v)}_{rs,Q} & u\neq v \\ \sum_{p\neq u} I^{(p,p)}_{rs,Q} & u = v \end{cases} \tag{14g}$$

where $I^{(u,v)}_{rs,Q}$ is given in terms of basic AO integrals as

$$I^{(u,v)}_{rs,Q} = 2\langle\chi_r|\frac{\mathscr{K}r_ur_v}{r^3_Q}|\chi_s\rangle + R_{Q,u}(R_{r,v}+R_{s,v})\langle\chi_r|\frac{\mathscr{K}}{r^3_Q}|\chi_s\rangle - (R_{r,v}+R_{s,v})\langle\chi_r|\frac{\mathscr{K}r_u}{r^3_Q}|\chi_s\rangle - 2R_{Q,u}\langle\chi_r|\frac{\mathscr{K}r_v}{r^3_Q}|\chi_s\rangle \tag{14h}$$

The matrix elements of eq 13c were implemented as follows:

$$R^{(u,v)}_{rs,Q} = \frac{1}{4}\{R_{sr,b}[B_{rs,mn,a} - B^{*}_{sr,mn,a} - (B_{rs,nm,a} - B^{*}_{sr,nm,a})] - R_{sr,a}[B_{rs,mn,b} - B^{*}_{sr,mn,b} - (B_{rs,nm,b} - B^{*}_{sr,nm,b}]\} - \frac{i}{2}(\boldsymbol{R}_r\times\boldsymbol{R}_s)_u H^{(v)}_{rs,Q} \tag{14i}$$

dx.doi.org/10.1021/ct200408j |J. Chem. Theory Comput. 2011, 7, 3278–3292

where *uab* = *xyz,yzx,zxy*; *vmn* = *xyz,yzx,zxy*; and $B_{rs,mn,a}$ is given as

$$B_{rs,\,mn,\,a} = \langle \chi_r | r_a \mathscr{K} \frac{r_{Q,\,m}}{r_Q^3} | \frac{\partial \chi_s}{\partial r_n} \rangle \tag{14j}$$

with $r_a = x,y,z$. Further, $\mathbf{R}_{sr} = \mathbf{R}_s - \mathbf{R}_r$.

Matrix elements for the spin−orbit operator derivative, eq 13e, needed for the Δg tensor are calculated as

$$H_{rs}^{(v)} = \frac{i}{2} \int \mathrm{d}^3 r (\mathscr{K} - 1)[\{\nabla \chi_r^*\} \times \{\nabla \chi_s\}] \tag{14k}$$

using AO integrals of the form $\langle (\partial \chi_r / \partial r_m) | \mathscr{K} - 1 | (\partial \chi_s / \partial r_n) \rangle$. In eq 14k, use is made of the fact that $\nabla \mathscr{K} \times \nabla = \nabla (\mathscr{K} - 1) \times \nabla$ in order to eliminate vanishing contributions.[35] For the bilinear perturbation operator, eq 13f, in the Δg tensor, matrix elements are calculated as

$$H_{rs}^{(u,v)} = -\frac{1}{4}[\delta_{uv} \sum_n (M_{rs,\,nn,\,s} + M_{sr,\,nn,\,s}^*) - (M_{rs,\,uv,\,s} + M_{sr,\,uv,\,s}^*)] \tag{14l}$$

with $M_{rs,uv,t}$ given as

$$M_{rs,\,uv,\,t} = \langle \frac{\partial \chi_r}{\partial r_u} | (\mathscr{K} - 1) r_{t,\,v} | \chi_s \rangle \tag{14m}$$

where $r_{t,v} = r_v - R_{t,v}$.

Finally, we have the matrix elements of eq 13g, which were implemented as

$$\begin{aligned} R_{rs}^{(u,v)} = & -\frac{1}{4}[R_{sr,\,b}[A_{rs,\,mn,\,a} - A_{sr,\,mn,\,a}^*] \\ & - R_{sr,\,a}[A_{rs,\,mn,\,b} - A_{sr,\,mn,\,b}^*] + \\ & \delta_{uv} \sum_n R_{sr,\,n} \langle \chi_r | (\mathscr{K} - 1) | \frac{\partial \chi_s}{\partial r_n} \rangle - R_{sr,\,v} \langle \chi_r | (\mathscr{K} - 1) | \frac{\partial \chi_s}{\partial r_u} \rangle] \\ & - \frac{i}{2} (\mathbf{R}_r \times \mathbf{R}_s)_u H_{rs}^{(v)} \end{aligned} \tag{14n}$$

with

$$A_{rs,\,mn,\,a} = \langle \frac{\partial \chi_r}{\partial r_m} | r_a (\mathscr{K} - 1) | \frac{\partial \chi_s}{\partial r_n} \rangle \tag{14o}$$

Equation sets 11, 12, 13, and 14 form the working expressions for the ZORA implementation of NMR shielding and Δg tensors in NWChem.

The formalism outlined here corresponds to "unscaled" ZORA computations. A "scaled" ZORA variant has been suggested by Wolff et al.[26] In the scaled ZORA approach, the shielding tensor is formulated in terms of a sum of derivatives of the Kohn−Sham orbitals φ_i and their energies ε_i. As was shown by van Lenthe,[72] the ZORA orbital energies of one-electron systems can be improved considerably toward the fully relativistic value by applying a scaling factor

$$\varepsilon_i^{\text{scaled-ZORA}} = S_i \varepsilon_i^{\text{ZORA}} \tag{15}$$

where, in a scalar relativistic ZORA framework

$$S_i = \left[1 + \langle \varphi_i | \hat{\mathbf{p}} \frac{c^2}{[2c^2 - V]^2} \hat{\mathbf{p}} | \varphi_i \rangle \right]^{-1} \tag{16}$$

The scaling factors can be conveniently included in the unperturbed and perturbed density matrices in eqs 8a and 8b.[50] For valence orbitals, which dominate the chemical shifts, the scaling factors are close to 1 and do not severely alter the results. Larger effects are generally obtained for core orbitals where the unscaled ZORA orbital energies and related terms in derivative properties are not very accurate.

3. COMPUTATIONAL DETAILS

The new implementation and computations reported herein are based on a 2011 developer's version of the open source NWChem package.[73−75] Recently developed ZORA functionality reported by Nichols et al.[37] and by us[50] has been utilized and extended for scalar ZORA linear response DFT computations as described in section 2. Consistent with a previous ZORA implementation of *g*-shifts as second order derivatives in the Amsterdam Density Functional (ADF) package,[38,35] spin−other-orbit (SOO) terms have been neglected since our main focus is on systems with heavy atoms. For a justification of this approximation, see ref 76. Finite nuclear models were not used for the present study.

Computations that were performed mainly to validate the NWChem ZORA-SR shielding module employed the set of diatomic molecules HX (X = F, Cl, Br, I, At) and the H_2X (X = O, S, Se, Te, Po) series. Geometries for HX and H_2X were obtained from refs 77 and 78, respectively. For the heavy atoms X, we employed a Gaussian-type atomic orbital (GTO) basis set with sufficient flexibility in the core region to be able to describe the scalar ZORA effects on the orbitals. The ANO-RCC basis sets by Roos et al.[79] in a fully uncontracted fashion were found to be suitable for this purpose (for a related ZORA benchmark of electric field gradients, see ref 50). For hydrogen, the TZVPP basis set by Weigend and Ahlrichs[80] was used. This and the other basis sets were downloaded from the EMSL basis set exchange.[81,82] A second set of calculations aimed at verifying the implementation was performed for a set of selected molecules containing tellurium. These systems have been used previously to explore scalar relativistic effects on NMR chemical shifts.[83−85] For the Te benchmark, we employed two sets of geometries: (a) geometries obtained from X-ray diffraction, as reported in ref 86 for $TeCl_4$, ref 87 for $TeF_2C_2F_6$, ref 88 for $TeMe_2Cl_2$, ref 89 for TeO_6H_6, ref 90 for TeF_6, ref 91 for $TeMe_2$, ref 92 for $TeMe_4$, and ref 93 for TeH_2; (b) optimized geometries obtained with ADF using the Becke88[94]+Perdew86[95] (BP) functional and a triple-ζ doubly polarized ZORA STO basis set (TZ2P). For the NWChem NMR calculations, we employed the uncontracted ANO-RCC basis set for tellurium and the 6-311G* Pople GTO basis set on the ligands. For comparison, ZORA-SR NMR computations were carried out with a developers version (pre-2011 release) of ADF using a quadruple-ζ multiply polarized (QZ4P) ZORA STO basis set for all atoms. For the validation and comparison with ADF, the following functionals were applied in the NMR computations: BP and the Becke three-parameter Lee−Yang−Parr (B3LYP) hybrid.[96] The performance of the NWChem ZORA-SR shielding module for the evaluation of ^{125}Te chemical shifts has been further tested by comparing calculated results with experimental data, using the functionals BP and B3LYP, and the standard parametrization of a Coulomb-attenuated (range separated) version of B3LYP,[48] denoted here as CAM-B3LYP-A or short:CAM-A. In this parametrization, the fraction of Hartree−Fock exchange at large electronic separations approaches $\alpha + \beta = 0.65$.

The calculations of the uranium(VI) chloride fluorides $UF_{6-n}Cl_n$ employed optimized geometries reported by Straka and Kaupp,[60] which were obtained with the B3LYP functional and a scalar relativistic effective core potential (ECP). We used the uncontracted ANO-RCC basis set for uranium, with *h* functions removed in order to save computational resources. A justification for removing these functions in DFT calculations has been provided in ref 50. Since for the U(VI) complexes the main interest is in the ligand NMR shielding, a basis set devised for calculations of magnetic properties, namely the IGLO-III basis,[97] has been used for F and Cl. For comparison with previously published work on these systems, the calculations employed the BP and B3LYP functionals as well as a global hybrid with 50% HF exchange, BHLYP. The performance of range-separated functionals was further tested with a parametrization of CAM-B3LYP denoted here as CAM-B where $\alpha + \beta = 1$ (fully long-range corrected), and a fully long-range corrected hybrid form[98] of the Perdew–Burke–Ernzerhof (PBE) functional,[95] which is denoted here as LC-PBE0.

The computations involving the NWChem ZORA-SR *g*-shifts module were carried out for a set of small radicals for which geometries were optimized with ADF using ZORA/BP/TZVP with the exception of CdF, HgCN, and HgAg, where we used optimized bond lengths from ref 99. For the members of the test set with less heavy atoms, viz., CH_2, CH_3, CHO, HSiO, HSiS, SiOH, and SiSH, the IGLO-III basis set was used. For the molecules with heavier atoms, viz., TiF_3, CdF, HgF, HgCN, HgF, HgAg, and NpF_6, the uncontracted ANO-RCC basis was used for Ti, Cd, Hg, Ag, and Np (with *h* functions removed for Ti and Np and *g* functions removed for Cd, Hg, and Ag) and IGLO-III for the other atoms. A second set of *g*-shifts computations was performed using the 6-311G** basis set in place of IGLO-III. For comparison, we computed g shifts using ADF with the TZ2P basis set and the following methodologies: (i) a recently implemented second derivative *g* shift code for STO basis sets discussed in ref 35 and (ii) the van Lenthe, Wormer, and van der Avoird (LWA) implementation in ADF[34] which calculates the *g* tensor as a first derivative, with SO coupling included variationally in the ground state. For the *g* shift benchmark, the following functionals were employed: PBE, a global hybrid based on PBE with 25% HF exchange (PBE0),[100,101] and CAM-A.

Default "extra fine" integration grids were used except for tellurium in tellurium complexes; uranium, fluorine, and chlorine in uranium halides; and neptunium and fluorine in NpF_6 where radial grids with additional points (350 radial grids in total) were used for better convergence of the numerical perturbation operator matrix elements. In the cases of HX, H_2X, and tellurium complexes, we checked the performance of the adopted numerical grid by comparing nonrelativistic shieldings obtained via analytical and numerical integration, respectively.

4. RESULTS AND DISCUSSION

4.1. Shielding of X in HX and H_2X. This section is mainly concerned with a validation of the ZORA-SR shielding implementation. Table 1 provides the relativistic effects obtained from scalar ZORA B3LYP computations of the heavy atom shielding constants for HX where X = F, Cl, Br, I, and At and for H_2X where X = O, S, Se, Te, and Po. The columns labeled as *nonrel* provide the calculated nonrelativistic shielding, which has been used to obtain the relativistic effects labeled as Δ(rel) by taking the difference of the relativistic and the nonrelativistic shielding.

Table 1. Comparison of Scalar Relativistic Effects Δ(rel) on Nuclear Shielding Obtained with NWChem[a] (Implementation Described in Section 2) and ADF[b]. B3LYP functional[c].

	σ_{iso} NWChem		σ_{iso} ADF	
system[d]	nonrel	Δ(rel)[e]	nonrel	Δ(rel)[e]
H_2O	326.5	−0.6	327.0	−0.6
H_2S	700.5	−4.9	700.4	−4.5
H_2Se	2084	−50.2	2084	−48.8
H_2Te	3547	−177.9	3549	−182.7
H_2Po	7080	−828.3	7080	−832.7
HF	411.3	−0.8	412.6	−0.8
HCl	938.1	−5.1	937.7	−5.0
HBr	2571	−44.0	2572	−43.2
HI	4433	−146.6	4434	−149.0
HAt	8451	−709.7	8453	−717.9

[a] Scaled ZORA-SR with uncontracted ANO basis for X and TZVPP for H. [b] Scaled ZORA-SR with QZ4P STO basis set for X and TZ2P for H. NMR implementation of Wolff et al.[26] [c] Computed shielding of X for H_2X (X = O, S, Se, Te, Po) and HX (X = F, Cl, Br, I, At). [d] Equilibrium geometries for HX and H_2X taken from refs 77 and 78. [e] $\Delta(\mathrm{rel}) = \sigma_{iso}^{SR} - \sigma_{iso}^{nonrel}$.

Although the ANO basis used for the heavy atoms X is not optimal for nonrelativistic calculations (in particular for the heaviest members of the series), its use in a fully uncontracted form should provide sufficient flexibility in order to obtain a reasonable estimate for the relativistic corrections. The same argument applies to the QZ4P Slater-type basis set used for the computations with ADF. Table S1 in the Supporting Information (SI) is similar to Table 1 but collects results obtained with the nonhybrid BP functional instead.

Overall, there is close agreement between the shielding constants calculated with the ZORA implementations in NWChem and those in the ADF program. The relativistic effects on the shielding constants generated by ZORA-SR are particularly close for the nonhybrid BP functional (see SI) but also very similar in the hybrid DFT calculations with the B3LYP functional. Differences between the two codes must be expected, most importantly due to the different nature of the basis sets (GTO versus STO, and details on how these basis sets were optimized) and the numerical integration grids used to calculate DFT-related XC contributions. Further, the HF exchange contributions in ADF are calculated via an orbital-pair density fitting procedure and therefore affected by the quality of the auxiliary density-fit basis sets that accompany the STO basis sets included in the ADF basis set library. Another contributing factor is how the potential in the denominator in $\mathscr{K}$, eq 5, is approximated: NWChem uses a sum of atomic nuclear and Hartree potentials, whereas ADF further includes a sum of approximate exchange-correlation potentials. Keeping these technical differences in mind, the agreement of the results obtained with the two ZORA implementations can be considered as excellent, showing that comparable relativistic effects in the shielding constants are generated. Considering, further, that calculations of chemical shifts tend to furnish cancellation of systematic errors such as those from numerical integration, the new implementation in NWChem is expected to predict very comparable chemical shifts to the one in ADF when using the same functionals and basis sets of comparable flexibility.

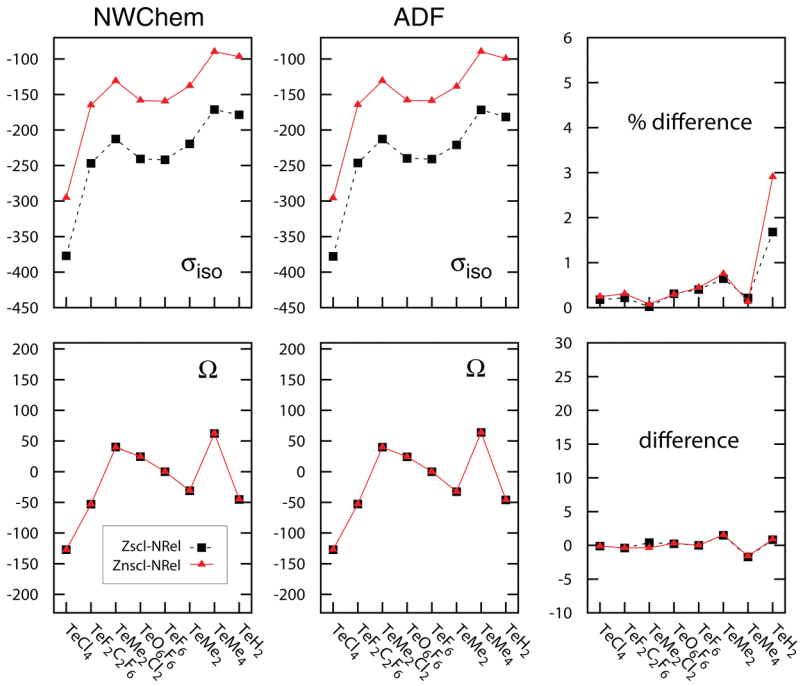

Figure 1. Comparison of relativistic effects (rel − nonrel) on ^{125}Te shielding constants and shielding tensor spans (Ω), in ppm. Calculations using the ZORA-SR shielding implementations in NWChem reported in this work, and the implementation by Wolff et al.[26] in the ADF program. Unscaled and scaled ZORA-SR, B3LYP functional.

Manninen et al.[102] have previously calculated relativistic effects of order c^{-2}, corresponding to the Breit−Pauli operator, on nuclear shielding of the HX and H_2X series directly as perturbations, using nonrelativistic HF and complete active space (CAS) MCSCF wave functions. The effects were divided into passive and active contributions, with the former originating from relativistic changes of the wave function and the latter from relativistic terms $\mathcal{O}(c^{-2})$ in the magnetic perturbation operators. A comparison of our results with those of Manninen et al. shows the following: (i) The nonrelativistic shieldings differ by about 3−7%, which must be attributed to basis set effects and the different treatment of correlation and exchange in the calculations. (ii) Regarding the relativistic effects on the X shielding, we considered the "passive" SR terms of Table 1 of ref 102 and a scalar relativistic (SR) "active" term from Table 3 but no terms involving the Fermi-contact and spin-dipole operators. The ZORA analogs of the latter contribute to the shielding in variational relativistic calculations with spin−orbit coupling included and will be the subject of a follow-up study. The sum of several passive scalar relativistic terms was calculated to be positive by Manninen et al. in ref 102 but shown to be sensitive to the basis set—in particular the augmentation with high exponents—and correlation. The sensitivity arises in part from a cancellation of perturbation terms of opposite sign, which in some cases individually exceed the total by more than an order of magnitude. An active orbital−Zeeman−kinetic energy term was calculated to be positive for the HX and H_2X series and shown to be relatively insensitive to correlation. The SR effects on the X shielding are calculated to be negative with ZORA DFT. However, Manninen et al. noted in ref 102 that a large negative active SR contribution to the shielding was neglected in the study. This and other previously neglected terms were later calculated explicitly, leading to additional large and negative SR contributions to the X shielding in the HX and H_2X series, which overpower the positive terms.[103] Given the sensitivity to correlation and the fact that the present ZORA calculations are variational, a direct comparison with the data by Manninen et al. is difficult. We therefore deem the excellent agreement with the ADF ZORA implementation and the overall sign of the SR effects on the X shielding as sufficient to validate the method. It is noted in passing that a set of perturbation terms corresponding to the Pauli approximation can be obtained from ZORA by using $\mathcal{K} \approx 1 + V/(2c^2)$ and applying partial integration or the turnover rule for the momentum operator in the matrix elements.

4.2. NMR Shielding and Chemical Shifts of Tellurium Compounds. Calculations for a set of selected tellurium compounds employed X-ray geometries taken from several references indicated in the Computational Details section and in the table footnotes. Figure 1 displays a graphical comparison of the scalar relativistic effects on isotropic Te shielding constants σ_{iso} and on the shielding tensor span Ω, calculated with the NWChem ZORA-SR implementation and with the ADF package using the B3LYP functional. The corresponding numerical data for the B3LYP and the BP functional, as well as a graphical comparison similar to that of Figure 1 but for BP computations, are provided in Tables S2 and S3 and in Figure S1 of the Supporting Information (SI). The calculations employed an unscaled as well as a scaled ZORA formalism, as outlined near the end of section 2.

The agreement between the NWChem and the ADF ZORA results seen in Figure 1 and the corresponding tables and the figure in the SI is very good. Further, the effects from the ZORA scaling are also very close. Reasons have already been provided in the previous section why minor differences must be expected between the calculations performed with NWChem and ADF. The results for the Te compounds show that the combination of the uncontracted ANO-RCC basis for the heavy atom with 6-311G* for lighter atoms provides a suitably flexible basis set

Table 2. ^{125}Te Chemical Shifts (ppm), ZORA-SR Calculations with NWChem[a] and Experimental Data

	BP		B3LYP		CAM-B3LYP			experimental	
system	opt[b]	X-ray[c]	opt[b]	X-ray[c]	opt[b]	X-ray[c]	ref 83[d]		
$TeCl_4$		1703		1612		1835	1541	1725	ref 104
TeC_2F_6	1379		1470		1804		1404	1368	ref 105
$TeF_2C_2F_6$	959	864	867	792	1256	1220		1187	refs 106 and 107
$TeMe_2Cl_2$	494	432	458	398	506	466	451	734	ref 108
TeO_6H_6	570	598	498	526	928	1008	614	707	ref 109
TeF_6	416	434	327	342	750	811	604	543	ref 110
$TeEt_2$	410		399		558		346	380	ref 111
$TeMe_2$	0	0	0	0	0	0	0	0	
$TeMe_4$	−292	−185	−326	−212	−303	−136	−280	−67	ref 112
TeH_2	−1008	−878	−964	−835	−983	−846	−770	−621	refs 111 and 113
Δ[e]	173	177	218	226	242	182	131		

[a] Scaled ZORA-SR with uncontracted ANO basis set for Te and 6-311G* basis set for C, H, F, and Cl. [b] Scalar ZORA optimized geometries obtained with ADF using the BP functional and the TZ2P basis set. [c] X-ray geometries obtained from ref 86 for $TeCl_4$, ref 87 for $TeF_2C_2F_6$, ref 88 for $TeMe_2Cl_2$, ref 89 for TeO_6H_6, ref 90 for TeF_6, ref 91 for $TeMe_2$, ref 92 for $TeMe_4$, ref 93 for TeH_2. [d] Quasirelativistic generalized Moller−Plesset perturbation theory (QR-GUMP2). Electron correlation included via MP2. The X-ray geometries for $TeCl_4$, $TeMe_2Cl_2$, TeO_6H_6, and TeH_2 are the same geometries used in our calculations. [e] Δ = unsigned mean deviation from experimental results.

for this type of calculation that should allow for routine applications in systems with one or a few truly heavy atoms (in the context of this and the following sections, atoms with nuclear charges less than about 20 to 30 may be considered light atoms). For calculations of ligand NMR shifts, it would be advisible to use basis sets designed for NMR shielding calculations for the ligand atoms. The comparison of unscaled and scaled ZORA results indicates that the main effect of the ZORA scaling is a relatively constant positive change of the isotropic shielding, which cancels to a large degree when evaluating chemical shifts. The effects on the tensor span are hardly noticeable on the scale of the plots. Noticeable effects on chemical shifts due to ZORA scaling are likely to be significant only for systems where the scaling factors deviate noticeably from unity for valence orbitals that are contributing to the shielding.

Table 2 collects tellurium chemical shifts calculated with optimized geometries and with geometries determined experimentally from X-ray diffraction. The tellurium chemical shifts, δ_{Te}, were obtained with dimethyl telluride, $TeMe_2$, as the reference, using $\delta_{Te} = \sigma_{TeMe_2} - \sigma_{compound}$. Table S4 of the SI provides the shielding constants calculated for the reference. Calculations were performed with the functionals BP, B3LYP, and CAM-B3LYP. The last column in the table lists corresponding experimental chemical shifts obtained in varying solvents. Solvent effects together with thermal motions have been estimated to contribute on the order of ±100 ppm to the experimental chemical shifts.[85,114] The data reveal several trends: (i) For the compounds with positive chemical shifts, there is a tendency for $\delta_{Te,B3LYP} < \delta_{Te,BP} < \delta_{Te,exp} < \delta_{Te,CAM}$. For example, for TeO_6H_6 for the optimized geometry, $\delta_{Te,B3LYP}$ = 498 ppm, $\delta_{Te,BP}$ = 570 ppm, $\delta_{Te,exp}$ = 707 ppm, and $\delta_{Te,CAM}$ = 928 ppm. It appears that CAM-B3LYP is overestimating these chemical shifts in the framework of scalar ZORA. (ii) For the compounds with negative chemical shifts, the X-ray geometries give results closer to experiment than the optimized geometries. For example, for $TeMe_4$, the closest agreement with experiment is $\delta_{Te,CAM}$ = −136 ppm as opposed to the "best" result based on the optimized geometry, $\delta_{Te,BP}$ = −292 ppm. (iii) The deviations between the DFT results and the quasi-relativistic MP2 data of ref 83 (which includes spin−orbit effects) are roughly of the same magnitude as deviations between the various sets of calculations and experimental results.

A comparison of calculated and experimental chemical shifts is provided in Figure 2. Overall, the predicted chemical shifts correlate reasonably well with experimental data for all three functionals. For most of the tellurium compounds, the predicted scalar relativistic CAM-B3LYP chemical shifts are slightly further away from experimental values than the corresponding nonrelativistic chemical shifts. Mean unsigned deviations of the scalar ZORA results from experimental results are listed in Table 2. The deviations range from 7% (BP functional) to 10% (CAM-B3LYP with optimized geometries) of the chemical shift range of the set of Te compounds, while the deviations for the MP2 literature data are slighly smaller on average (6% of the chemical shift range). The CAM-B3LYP data calculated with the experimental geometries have similar deviations from experimental results as both sets of BP functional data. On the scale of the chemical shift range, the overall performance of the different functionals is roughly comparable. Substantial and systematic improvements of the DFT calculations should further include solvent effects and spin−orbit terms in the shielding tensors.

4.3. Shielding of Uranium(IV) Chloride Fluoride Complexes. Table 3 collects scalar relativistic ^{19}F shielding constants for a set of uranium(VI) halide complexes. The fluorine shieldings calculated with the BP and B3LYP functionals are very close to those obtained by Straka and Kaupp,[60] which are listed in Table 3 in parentheses. Straka and Kaupp employed a small-core relativistic effective core potential (RSC ECP) as opposed to our all-electron scalar ZORA approach. Since the calculations are performed for the shielding of a light nucleus in heavy atom compounds, the two approaches are expected to yield comparable results. It is reassuring that this is indeed the case. We note that the present ZORA-SC computations were carried out with B3LYP/RSC-TZVP optimized geometries taken from ref 60. The optimized bond lengths are very similar to those reported by Schreckenbach.[62] Table 3 also lists results obtained by Straka and Kaupp with the BHLYP functionals, which overall agreed best

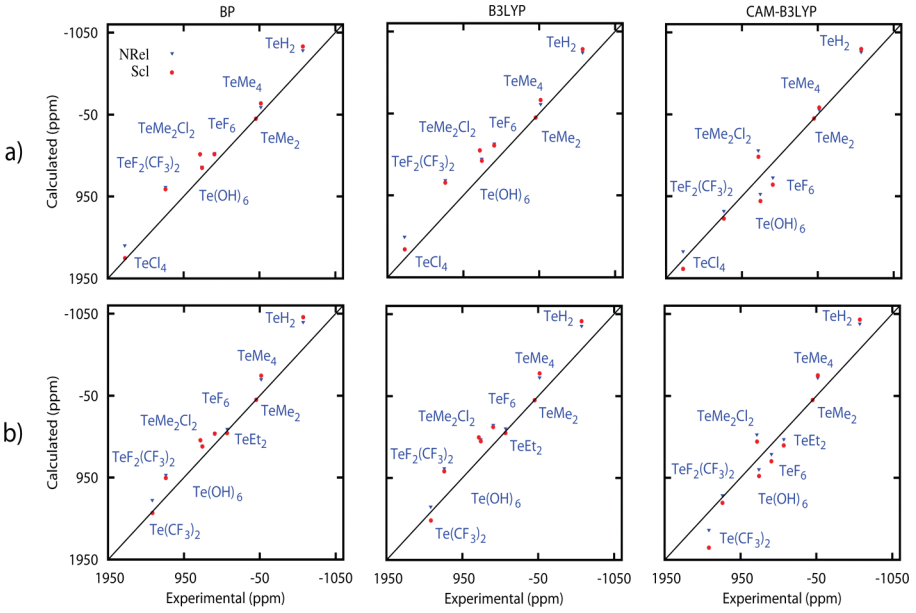

Figure 2. Performance of BP, B3LYP, and CAM-B3LYP functionals for ^{125}Te chemical shifts calculated (a) with X-ray crystallographic geometries and (b) with optimized geometries. NWChem, scaled ZORA-SR. The 45° lines indicate where $\delta_{calcd} = \delta_{exptl}$.

Table 3. Dependence of ^{19}F Shielding in UF_nCl_{6-n} ($n = 1-6$)[a] on the XC Functional[b]

system	position[c]	BP		B3LYP		BHLYP	BHH	CAM-A	CAM-B	LC-PBE0	experimental[60]
UF_6	F_{tF}	−720.3	(−727.0)	−697.9	(−706.2)	(−606.7)	−604.4	−644.6	−604.1	−611.8	−575.3
UF_5Cl	F_{tF}	−712.0	(−714.6)	−689.2	(−692.6)	(−606.2)	−612.8	−647.1	−614.2	−628.2	−573.3
trans-UF_4Cl_2	F_{tF}	−706.8	(−705.9)	−685.0	(−684.2)	(−611.1)	−625.2	−652.0	−625.7	−645.5	−566.8
cis-UF_4Cl_2	F_{tF}	−705.0	(−705.1)	−682.5	(−682.7)	(−606.7)	−619.4	−648.4	−621.2	−640.2	−571.3
mer-UF_3Cl_3	F_{tF}	−701.7	(−699.7)	−680.3	(−678.0)	(−613.0)	−630.9	−653.1	−631.0	−654.7	−564.3
trans-UF_2Cl_4	F_{tF}	−699.0	(−695.9)	−679.3	(−675.6)	(−620.0)	−641.2	−657.1	−639.1	−666.5	−557.4
$UFCl_5$	F_{tCl}	−652.5	(−647.8)	−659.9	(−655.5)	(−645.2)	−664.6	−652.0	−644.7	−675.6	−585.6
UF_5Cl	F_{tCl}	−679.6	(−682.0)	−683.2	(−689.0)	(−629.0)	−625.6	−644.7	−612.8	−623.8	−592.8
cis-UF_4Cl_2	F_{tCl}	−668.0	(−667.6)	−671.2	(−672.9)	(−627.5)	−632.3	−643.3	−619.5	−636.7	−597.1
mer-UF_3Cl_3	F_{tCl}	−662.0	(−659.1)	−666.5	(−664.7)	(−635.8)	−647.7	−647.7	−631.3	−654.4	−593.9
fac-UF_3Cl_3	F_{tCl}	−659.9	(−657.6)	−663.4	(−662.6)	(−628.2)	−638.8	−643.2	−625.5	−647.6	−597.7
cis-UF_2Cl_4	F_{tCl}	−655.6	(−651.8)	−660.9	(−657.8)	(−636.7)	−652.6	−647.7	−635.8	−662.8	−592.3

[a] Using scaled scalar ZORA with uncontracted ANO basis set for uranium and IGLO-III for fluorine and chlorine. [b] The data in parentheses correspond to calculations reported in ref 60. CAM-A = CAM-B3LYP-A, original parametrization ($\alpha + \beta = 0.65$), *CAM-B* = CAM-B3LYP-B, fully long-range-corrected parametrization ($\alpha + \beta = 1$), BHH = BeckeHandH, 50% HF exchange + 50% Slater exchange + 50% PW91LDA correlation. [c] F_{tF} = fluorine *trans* to another fluorine. F_{tCl} = fluorine *trans* to chlorine.

with experimental results. Because of the good agreement of our BP and B3LYP data with those of Straka and Kaupp, we decided to forego additional BHLYP computations and focus on the range-separated functional instead. Results from calculations with another 50% global hybrid, the Becke "half and half" parametrization (BHH), are additionally listed in Table 3. A visual comparison of the results with experimental data is shown in Figure 3. Experimental absolute shieldings were taken from ref 60. The graph in Figure 3 has been designed to appear similar to a graph in ref 60, which we found very suitable for illustrating the various trends in the data set.

As outlined in the Computational Details, the performance of three long-range corrected functionals has been tested. Among those, CAM-B3LYP in its fully long-range corrected form (CAM-B) gives calculated shieldings that are closest to experimental results, with LC-PBE0 being close in some cases and more similar to CAM-A in others. For the example mentioned in the Introduction, *mer*-UF_3Cl_3, the CAM as well as the LC-PBE0 calculations yield F_{tCl} and F_{tF} to be approximately equal. This is an improvement over BP and B3LYP, which give substantially smaller magnitudes for F_{tCl} vs F_{tF}, whereas the experimental data show the opposite trend. The improvement with the long-range corrected functionals is not as strong as it is with BHLYP, which, for *mer*-UF_3Cl_3, gives a 23 ppm more positive shielding for F_{tF} vs F_{tCl}. Our calculations with the Becke half-and-half functional also reproduce this trend. Overall, the BP and B3LYP functionals appear to somewhat better reproduce the trend visible in Figure 3 within the F_{tF} group, unlike BHLYP and the range-separated functionals. However, BP and B3LYP fail to produce the overall larger shielding magnitudes in this group compared to F_{tCl}.

Beyond a comparison of their performance, a detailed analysis of how exactly the various approximations in the XC functionals

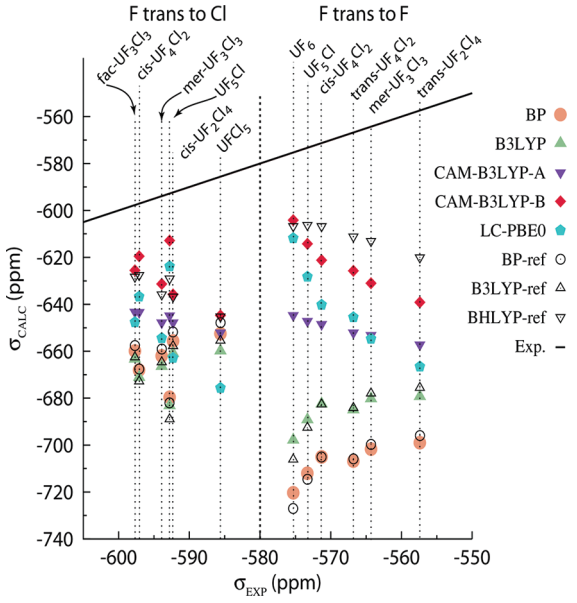

Figure 3. Performance of different functionals in the calculation of ^{19}F shielding in the UF_nCl_{6-n} (n = 1−6) series. BP-ref, B3LYP-ref, and BHLYP-ref are results from ref 60. The calculations used scaled ZORA-SR.

applied in this work influence the ^{19}F shieldings in the U(VI) halides is beyond the scope of this work. The comparison of the functionals already indicates that the fraction of HF exchange in the functional, and the balance of electron correlation with self-interaction and asymptotic behavior of the potential that it entails, influences various trends within the data set and the overall magnitude of the absolute shielding in different ways. A full long-range correction is evidently not beneficial in conjunction with the XC functionals applied in this study. B3LYP appears to have a too small fraction of HF exchange to provide a substantial difference over the nonhybrid BP functional for the U(VI) halides. Given the fact that the global 50% hybrid BHLYP previously gave the best overall performance, giving larger magnitudes of F_{tF} versus F_{tCl} shieldings, and considering that the standard parametrization of CAM-B3LYP only goes to 65% HF exchange at large interelectronic distances, one might have expected the CAM-A functional to perform well for this challenging set of chemical shifts. However, while the shielding constants overall are closer to experimental results (compared to BP and B3LYP), a clear trend for F_{tCl} vs F_{tF} is not obtained with this parametrization. Spin−orbit effects were previously shown to be too small to reconcile the differences between nonhybrid DFT calculations and experimental results.[62] Spin−orbit and other relatively minor effects may help to close the remaining gaps between some of the hybrid DFT calculations and experimental results. An evaluation of range-separated functionals in spin−orbit ZORA NMR calculations, and the inclusion of solvent effects, is planned for a follow-up study.

Schreckenbach has previously provided theoretical estimates for ^{235}U chemical shifts[62] based on all-electron scalar ZORA computations with nonhybrid functionals as implemented in ADF, indicating a large shift range that may exceed 20 000 ppm. For completeness, Table S5 in the Supporting Information provides the uranium shielding constants and tensor spans for the UF_nCl_{6-n} series. The agreement of the nonhybrid BP results with those from Schreckenbach's paper is quite close, which may serve as further validation of the NWChem implementation. The shielding constants are clearly dominated by negative paramagnetic contributions. The results serve as benchmark data only since physically meaningful absolute shieldings for U should be calculated with spin−orbit coupling and with a finite nucleus model. Regarding different functionals, we note that with the range-separated hybrid functionals, and in particular with the full LR corrected versions, the shielding constants become significantly more positive.

4.4. *g*-Shifts of Small Radicals. Data in Table 4 illustrate the performance of the NWChem ZORA *g* shift module for predicting *g*-shifts for a set of selected small radicals. A comparison is made with a second-order ZORA implementation in ADF that was recently reported in ref 35 ("AP", spin−orbit coupling treated as a perturbation, similar to the present NWChem implementation). Further, a comparison is made with ADF ZORA calculations using a first-order derivative approach developed by van Lenthe, Wormer, and van der Avoird (LWA). In these calculations, spin−orbit coupling is included variationally in the ground state calculations, see also ref 64. The TZ2P basis set has been used for the ADF calculations since acceptable agreement with experimental results has been obtained in previous works using this STO basis.[34,35,99] The test set allows for a comparison of the influence of nuclear charges (lighter to heavier elements) and different bonding situations. Table 4 compares different types of functionals and includes results obtained with the standard parametrization of CAM-B3LYP (CAM-A). The agreement of the second-order and first-order ZORA approaches is reasonably close except for the heavy atomic systems with rotational symmetry. This behavior is expected and has been discussed in detail elsewhere.[55,65,99] The second-order approaches tend to underestimate the magnitude of the isotropic *g* shift for such systems because the tensor component parallel to the rotational axis is suppressed. TiF_3 is one of the systems where hybrid functionals offer a clear improvement, in line with previous studies.[10] Atoms with tightly bound lone pairs (fluorine) and the notoriously difficult treatment of response properties in systems with 3d metals tend to benefit from hybrid functionals. For NpF_6, the *g* shift also increases significantly in magnitude when going from the nonhybrid GGA to the hybrid functionals. In the NWChem calculations, this brings the result closer to the experimental *g* shift derived from solid state data.[122] Regarding the performance of CAM-B3LYP, in comparison with the changes when going from PBE to PBE0 and in comparison with the differences between calculations and experimental results, the results are in most cases very similar to those obtained with the global hybrid PBE0. Overall, the range-separated hybrid does not appear to outperform the PBE0 global hybrid for the *g*-shifts of the few-atomic radical test set of Table 4. During the course of this study, we noticed that the diamagnetic *g*-shifts exhibited some sensitivity to the approximations used for $\mathscr{K}$ (eq 5). For example, for the molecule HSiS, the diagonal elements of the diamagnetic *g* shift tensor calculated with NWChem were (−0.0154, −0.0347, −0.0147) ppt (BP functional, unscaled ZORA), whereas the calculation with ADF gave (−0.0359, −0.0626, −0.0400) ppt. It was found that the difference is most likely due to the exclusion of the atomic XC potentials in V in the construction of $\mathscr{K}$ in NWChem, unlike in ADF where they are included. A comparison was made between the two codes, using in both cases only the nuclear potentials in the construction of $\mathscr{K}$. In this case, the diagonal elements of the diamagnetic *g* shift tensor for molecule HSiS were calculated as (−0.475, −0.552, −0.528) ppt and

Table 4. Calculated Δg Shifts for Selected Molecules in ppt[a]

	NWChem			ADF (AP)[b]		ADF (LWA)[b]	exptl.
system[c]	PBE	PBE0	CAM-A	PBE	PBE0	PBE	
CH_2	0.1824	0.1674	0.1819	0.2057	0.1917	0.1383	
CH_3	0.5084	0.4763	0.5160	0.5380	0.5080	0.4733	0.10[d]
CHO	−3.028	−3.084	−3.184	−2.333	−2.298	−2.442	−2.1[e]
HSiO	−1.704	−1.552	−1.440	−1.696	−1.539	−1.820	−1.3[f]
HSiS	−1.526	−1.322	−0.2505	−1.646	−1.463	−1.895	
SiOH	−23.83	−25.18	−35.47	−24.13	−25.83	−24.13	
SiSH	−13.57	−14.44	−17.93	−14.03	−15.12	−14.09	
TiF_3	−29.20	−41.26	−43.44	−28.16	−39.94	−28.54	−77.92[g]
CdF	−11.92	−10.84	−10.69	−11.50	−10.45	−10.32	−9.667[h]
HgH	−97.85	−95.05	−99.82	−93.84	−91.66	−131.0	−125[i]
HgCN	−55.25	−55.87	−57.97	−53.76	−54.58	−78.13	
HgF	−17.21	−12.86	−10.09	−17.48	−13.02	−31.55	−30.7[j]
HgAg	−64.96	−64.18	−61.20	−61.58	−60.56	−80.28	−59.00[k]
NpF_6	−1795	−2359	−2299	−2761	−3015	−2564	−2606[l]

[a] Result in parts per thousand. NWChem calculations with uncontracted ANO basis for Ti, Cd, Hg, Ag, and Np and IGLO-III for other atoms. ADF calculations with STO basis set TZ2P. Both calculations used unscaled ZORA-SR. CAM-A = CAM-B3LYP, original parametrization ($\alpha + \beta = 0.65$). AP = ADF calculations with ZORA second-derivative approach similar to the present NWChem implementation, developed by Autschbach and Pritchard.[35] LWA = ADF calculations with ZORA first-order approach including spin-orbit coupling variationally, as developed by van Lenthe et al.[34] [b] CdF, HgCN, and HgAg were calculated using AP and LWA implementations in ADF. Data for the other molecules were taken from ref 35. [c] All systems calculated as doublets except triplet CH_2. Optimized geometries obtained with ADF using ZORA/BP/TZ2P with the exception of CdF, HgCN, and HgAg, for which optimized bond lengths were taken from ref 99. [d] Ref 115. [e] Ref 116. [f] Ref 117. [g] Ref 118. [h] Ref 119. [i] Ref 120. [j] Ref 121. [k] Ref 122. [l] Ref 123. Regarding NpF_6, see text and SI for further details.

(−0.469, −0.556, −0.521) ppt with NWChem and ADF, respectively. These results agree much better. Due to the very small magnitude of Δg^{dia}, the overall results are not strongly impacted by this sensitivity.

The comparison of the NWChem GTO basis calculations to the ADF results calculated with an STO basis set shows very similar trends for the functionals and overall a close agreement, with the exception of NpF_6. Calculations performed for this system with only the nuclear potential used in the construction of $\mathscr{K}$ produced significantly more negative g-shifts (changes on the order of -10^3 ppt, PBE functional) but the differences between the GTO and STO basis calculations remained. Table S6 of the Supporting Information is similar to Table 4 except that the NWChem results were obtained with the 6-311G** basis in place of IGLO-III for light atoms. The comparison of the data in the two tables shows that the GTO basis results are very close. Additional calculations with the PBE0 functional and the GTO basis sets 6-311++G** and aug-cc-pVDZ for fluorine yielded an isotropic g shift of −2370 and −2357 ppt, respectively, for NpF_6. These values are very close to the g-shifts listed in Tables 4 and S6. Hence, these calculations do not indicate a very pronounced fluorine basis set dependence of the NpF_6 g shift. Further, a calculation for NpF_6 (PBE functional) gave differences of only a few parts per thousand upon removal of the g functions from the Np ANO basis. Calculations with varying fluorine STO basis sets, going from an unpolarized double-ζ (DZ) to a large triply polarized quadruple-ζ basis (QZ4P), caused changes of less than −100 ppt. Overall, calculations with varying quality STO and GTO basis sets of varying sizes did not produce large enough changes to reconcile the g shift of NpF_6 calculated with the different codes.

We note that STOs used reach further into the asymptotic region than GTOs, and therefore the coverage of more diffuse regions by the basis set might be of some significance. The addition of diffuse p functions to the IGLO-III fluorine GTO basis did, however, not significantly change the calculated NpF_6 g factor. The TZ2P basis used for the STO calculations has one set of d and f polarization functions each for fluorine. In comparison, the IGLO-III basis for fluorine has two sets of d functions but no f. A test calculation with the TZVPP GTO basis for fluorine, which includes an f polarization function, gave a g shift of −1806 ppt (PBE functional). This result is not much different from the IGLO-III value of Table 4. A characterization of the frontier orbitals showed that the NWChem and ADF calculations converged to the same ground state.

The GTO based NWChem implementation does not approximate the Coulomb and exchange Fock matrix contributions beyond the approximations posed by the finite GTO basis set (and the density functional). On the other hand, in the ADF calculations, the Coulomb and XC potential and the HF exchange matrix are calculated by using an auxiliary density fitting basis which is limited to angular momenta of $l \leq 4$. Since the spin density of NpF_6 stems from the formal Np $5f^1$ configuration, the limitation of the angular momentum is of more concern for this system than for the other molecules in the test set. For the Coulomb and HF exchange, there is presently no alternative way of performing the ADF calculations. For the pure-DFT XC Fock matrix elements, however, it is possible to use the "exact" density represented in the AO basis instead of the fitted density. A series of such calculations (Table S7, SI) showed a significant decrease in the magnitude of the NpF_6 g factor, with the STO basis results obtained this way being closer to the GTO basis results. Quantitative agreement may therefore be expected if the fit-related limitations for the Coulomb and exact exchange Fock matrices are lifted. At present, the hybrid DFT GTO data obtained with the implementation reported herein (section 2) must be considered as the most reliable ZORA results.

5. SUMMARY AND OUTLOOK

Comparisons between ZORA calculations performed with the ADF code and Slater-type orbitals, and the new Gaussian basis ZORA NMR/EPR implementation in NWChem, using nonhybrid and standard global hybrid functionals, have shown good agreement and therefore serve as a validation of the new implementation. The calculation of the required ZORA perturbation operator matrix elements by numerical integration is rather straightforward. For *g*-shifts, good performance was found both for the PBE0 hybrid (25% HF exchange globally) and for the CAM-B3LYP range-separated hybrid. Range-separated hybrid functionals show some promise for NMR shielding calculations for difficult situations such as the ^{19}F shielding in the $UF_{6-n}Cl_n$ series of complexes, but it is possible that a universal setting for the range-separation parameter is limiting the performance of this class of functionals. The obvious next step is to calculate the fluorine shieldings of these systems with range-separated hybrids within a spin−orbit ZORA NMR framework, and with inclusion of solvent effects in order to more closely model the experimental conditions. Developments to enable spin−orbit ZORA NMR computations are currently under way in our team. Although previous work on the U(VI) halide series did not indicate that spin−orbit effects are able to bridge the large gap between nonhybrid DFT results and experiment al results,[62] they may further improve results with range-separated functionals and global hybrids with high fractions of HF exchange. As pointed out already, the agreement with experimental results is not ideal.

APPENDIX: ATTENUATED TWO-ELECTRON INTEGRALS USING THE RYS SCHEME

For completeness, we provide the details for the evaluation of the two-electron integrals in conjunction with range-separated functionals. In the range-separated approach, the electron repulsion is separated into long- and short-range parts. Since the NMR implementation[40] in NWChem is based on the Rys quadrature method,[123,124] we present the necessary changes for the modified two-electron integrals for attenuated interactions within this approach. The general form of the four-center, two-electron electron repulsion integral (ERI) is defined as

$$\left(\chi_i\chi_j\left|\frac{1}{r_{12}}\right|\chi_k\chi_l\right) = \int\int \chi_i(\mathbf{r}_1)\,\chi_j(\mathbf{r}_1)\frac{1}{r_{12}}\chi_k(\mathbf{r}_2)\,\chi_l(\mathbf{r}_2)\,\mathrm{d}^3r_1\,\mathrm{d}^3r_2 \tag{A-1}$$

where the $\chi_{i,j,k,l}$ are Gaussian primitive basis functions. Within the Rys scheme, the above integral is redefined as follows:

$$\left(\chi_i\chi_j\left|\frac{1}{r_{12}}\right|\chi_k\chi_l\right) = \frac{2}{\sqrt{\pi}}\int_0^\infty \mathrm{d}u(\chi_i\chi_j|\mathrm{e}^{-u^2r_{12}^2}|\chi_k\chi_l) \tag{A-2}$$

and similarly, the attenuated ERI can be written as

$$\left(\chi_i\chi_j\left|\frac{\mathrm{erf}(\gamma r_{12})}{r_{12}}\right|\chi_k\chi_l\right) = \frac{2}{\sqrt{\pi}}\int_0^\gamma \mathrm{d}u(\chi_i\chi_j|\mathrm{e}^{-u^2r_{12}^2}|\chi_k\chi_l) \tag{A-3}$$

by using $\mathrm{erf}(\gamma r_{12}) = \int_0^{\gamma r_{12}} \mathrm{e}^{-t^2}\,\mathrm{d}t$ and a variable change, $u = t/r_{12}$. After a further change of variables $t^2 = u^2/(\rho + u^2)$ and $1/\rho = 1/(a_i + a_j) + 1/(a_k + a_l)$, eq A-2 becomes

$$\left(\chi_i\chi_j\left|\frac{1}{r_{12}}\right|\chi_k\chi_l\right) = \int_0^1 P_L(t)\,\mathrm{e}^{-Xt^2}\,\mathrm{d}t \tag{A-4}$$

where P_L is a polynomial of degree L in t^2 and $X = \rho|r_A - r_B|^2$, and A and B are the centers of the orbital products ij and kl, respectively. X implicitly depends on the Gaussian exponents a_i, a_j, a_k, and a_l via ρ and the coordinates of the centers of the four Gaussians involved in the integral. The integral over t can be evaluated using an N point quadrature formula such as

$$\left(\chi_i\chi_j\left|\frac{1}{r_{12}}\right|\chi_k\chi_l\right) = \sum_{\alpha=1}^{N} P_L(t_\alpha)W_\alpha \tag{A-5}$$

where W_α is a weight factor. Similarly, the attenuated ERI in this approach becomes

$$\left(\chi_i\chi_j\left|\frac{\mathrm{erf}(\gamma r_{12})}{r_{12}}\right|\chi_k\chi_l\right) = \int_0^\beta P_L(t)\,\mathrm{e}^{-Xt^2}\,\mathrm{d}t \tag{A-6}$$

where $\beta = \gamma/(\rho + \gamma^2)^{1/2}$. In order to use the Rys formulas directly, we need another transform $t' = t/\beta$, to obtain

$$\left(\chi_i\chi_j\left|\frac{\mathrm{erf}(\gamma r_{12})}{r_{12}}\right|\chi_k\chi_l\right) = \int_0^1 P_L(t'\beta)\,\mathrm{e}^{-X\beta^2t'^2}\beta\,\mathrm{d}t' \tag{A-7}$$

which can be mapped directly onto eq A-5 with suitably modified weights and variables.

ASSOCIATED CONTENT

Supporting Information. X shielding constants for the HX series and tellurium shielding tensor data calculated with the BP functional. Numerical data used for Figure 1. Analog of Figure 1 but for the BP functional. Te reference shielding constants. Calculated U shielding tensor data. *g*-shifts calculated with different basis sets. This information is available free of charge via the Internet at http://pubs.acs.org.

AUTHOR INFORMATION

Corresponding Author
*E-mail: jochena@buffalo.edu.

ACKNOWLEDGMENT

This work has received financial support from the U.S. Department of Energy, grant no. DE-SC0001136 (BES Heavy Element Chemistry Program). We thank the Center for Computational Research (CCR) at the University at Buffalo for continuing support of our research projects. A portion of the research was performed using EMSL, a national scientific user facility sponsored by the U.S. Department of Energy's Office of Biological and Environmental Research located at Pacific Northwest National Laboratory (PNNL). PNNL is operated for the Department of Energy by the Battelle Memorial Institute under Contract DE-AC06-76RLO-1830. N.G. thanks M. Dupuis and W. A. de Jong for useful discussions and would like to acknowledge the DOE BES Heavy Element Chemistry Program (PI: De Jong, PNNL) of the

U.S. Department of Energy, Office of Science, and NWChem development for support.

REFERENCES

(1) Helgaker, T.; Jaszuński, M.; Ruud, K. *Chem. Rev.* **1999**, *99*, 293–352.

(2) Malkin, V. G.; Malkina, O. L.; Eriksson, L. A.; Salahub, D. R. The calculation of NMR and ESR spectroscopy parameters using density functional theory. In *Modern Density Functional Theory: A Tool for Chemistry*; Seminario, J. M., Politzer, P., Eds.; Elsevier: Amsterdam, 1995; Vol. 2.

(3) Facelli, J. C. Shielding Calculations. In *Encyclopedia of Nuclear Magnetic Resonance*; Grant, D. M., Harris, R. K., Eds.; John Wiley & Sons: Chichester, U. K., 2002; Vol. 9.

(4) Kaupp, M. Ab initio and density functional calculations of electronic g-tensors for organic radicals. In *EPR Spectroscopy of Free Radicals in Solids. Trends in Methods and Applications*; Lund, A., Shiotani, M., Eds.; Kluwer: Dordrecht, The Netherlands, 2002.

(5) Autschbach, J.; Ziegler, T. *Coord. Chem. Rev.* **2003**, *238/239*, 83–126.

(6) Autschbach, J. Relativistic effects on magnetic resonance parameters and other properties of inorganic molecules and metal complexes. In *Relativistic Methods for Chemists*; Ishikawa, J., Barysz, M., Eds.; Springer: London, 2010; Vol. 10.

(7) Kaupp, M.; Bühl, M.; Malkin, V. G. *Calculation of NMR and EPR Parameters. Theory and Applications*; Wiley-VCH: Weinheim, Germany, 2004.

(8) Rieger, P. H. *Electron spin resonance. Analysis and interpretation*; The Royal Society of Chemistry: Cambridge, U.K., 2007; p 3.

(9) Moon, S.; Patchkovskii, S. First−principles calculations of paramagnetic NMR shifts. In *Calculation of NMR and EPR Parameters. Theory and Applications*; Kaupp, M., Bühl, M., Malkin, V. G., Eds.; Wiley-VCH: Weinheim, Germany, 2004.

(10) Kaupp, M.; Köhler, F. H. *Coord. Chem. Rev.* **2009**, *253*, 2376–2386.

(11) Bertini, I.; Turano, P.; Vila, A. J. *Chem. Rev.* **1993**, *93*, 2833–2932.

(12) Rastrelli, F.; Bagno, A. *Chem.—Eur. J.* **2009**, *15*, 7990–8004.

(13) Autschbach, J.; Zheng, S. *Annu. Rep. NMR Spectrosc.* **2009**, *67*, 1–95.

(14) Nomura, Y.; Takeuchi, Y.; Nakagawa, N. *Tetrahedron Lett.* **1969**, *8*, 639–642.

(15) Kaupp, M.; Malkin, V. G.; Malkina, O. L.; Salahub, D. R. *J. Am. Chem. Soc.* **1995**, *117*, 1851−1852; Erratum *ibid.*, p. 8492.

(16) Schreckenbach, G.; Wolff, S. K.; Ziegler, T. Covering the entire periodic table: Relativistic density functional calculations of NMR chemical shifts in diamagnetic actinide compounds. In *Modeling NMR Chemical Shifts*; Facelli, J. C., de Dios, A. C., Eds.; American Chemical Society: Washington, DC, 1999; ACS Symposium Series 732.

(17) Kaupp, M.; Malkin, V. G.; Malkina, O. L. NMR of transition metal compounds. In *Encyclopedia of Computational Chemistry*; von Ragué Schleyer, P., Ed.; John Wiley & Sons: Chichester, U. K., 1998.

(18) Kaupp, M. Relativistic effects on NMR chemical shifts. In *Relativistic Electronic Structure Theory*; Schwerdtfeger, P., Ed.; Elsevier: Amsterdam, 2004; Vol. 2.

(19) Autschbach, J. Calculation of heavy-nucleus chemical shifts: Relativistic all-electron methods. In *Calculation of NMR and EPR Parameters. Theory and Applications*; Kaupp, M., Bühl, M., Malkin, V. G., Eds.; Wiley-VCH: Weinheim, Germany, 2004.

(20) van Lenthe, E.; Baerends, E. J.; Snijders, J. G. *J. Chem. Phys.* **1993**, *99*, 4597–4610.

(21) van Lenthe, E.; Ehlers, A.; Baerends, E. J. *J. Chem. Phys.* **1999**, *110*, 8943–8953.

(22) Wolf, A.; Reiher, M.; Hess, B. Transgressing theory boundaries: The generalized Douglas−Kroll transformation. In *Recent Advances in Relativistic Molecular Theory*; Hirao, K., Ishikawa, Y., Eds.; World Scientific: Singapore, 2004; Vol. 5.

(23) Fukuda, R.; Hada, M.; Nakatsuji, H. *J. Chem. Phys.* **2003**, *118*, 1015–1026.

(24) Malkin, I.; Malkina, O. L.; Malkin, V. G.; Kaupp, M. *J. Chem. Phys.* **2005**, *123*, 244103–16.

(25) Visscher, L.; Enevoldsen, T.; Saue, T.; Jensen, H. J. A.; Oddershede, J. *J. Comput. Chem.* **1999**, *20*, 1262–1273.

(26) Wolff, S. K.; Ziegler, T.; van Lenthe, E.; Baerends, E. J. *J. Chem. Phys.* **1999**, *110*, 7689–7698.

(27) Bouten, R.; Baerends, E. J.; van Lenthe, E.; Visscher, L.; Schreckenbach, G.; Ziegler, T. *J. Phys. Chem. A* **2000**, *104*, 5600–5611.

(28) Krykunov, M.; Ziegler, T.; van Lenthe, E. *J. Phys. Chem. A* **2009**, *113*, 11495–11500.

(29) Autschbach, J.; Ziegler, T. *J. Chem. Phys.* **2000**, *113*, 936–947.

(30) Autschbach, J.; Ziegler, T. *J. Chem. Phys.* **2000**, *113*, 9410–9418.

(31) Autschbach, J. *J. Chem. Phys.* **2008**, *129*, 094105–9. Erratum *ibid.***2009**, *130*, 209901.

(32) Autschbach, J. *ChemPhysChem* **2009**, *10*, 2274–2283.

(33) Moncho, S.; Autschbach, J. *J. Chem. Theory Comput.* **2010**, *6*, 223–234.

(34) van Lenthe, E.; Wormer, P. E. S.; van der Avoird, A. *J. Chem. Phys.* **1997**, *107*, 2488–2498.

(35) Autschbach, J.; Pritchard, B. *Theor. Chem. Acc.* **2011**, *129*, 453–466.

(36) Faas, S. *The ZORA approach in ab initio quantum chemistry*, Ph.D. Thesis, Rijksuniversiteit Groningen, The Netherlands, 2000.

(37) Nichols, P.; Govind, N.; Bylaska, E. J.; de Jong, W. A. *J. Chem. Theory Comput.* **2009**, *5*, 491–499.

(38) Baerends, E. J.; Ziegler, T.; Autschbach, J.; Bashford, D.; Bérces, A.; Bickelhaupt, F. M.; Bo, C.; Boerrigter, P. M.; Cavallo, L.; Chong, D. P.; Deng, L.; Dickson, R. M.; Ellis, D. E.; van Faassen, M.; Fan, L.; Fischer, T. H.; Fonseca Guerra, C.; Ghysels, A.; Giammona, A.; van Gisbergen, S. J. A.; Götz, A. W.; Groeneveld, J. A.; Gritsenko, O. V.; Grüning, M.; Gusarov, S.; Harris, F. E.; van den Hoek, P.; Jacob, C. R.; Jacobsen, H.; Jensen, L.; Kaminski, J. W.; van Kessel, G.; Kootstra, F.; Kovalenko, A.; Krykunov, M. V.; van Lenthe, E.; McCormack, D. A.; Michalak, A.; Mitoraj, M.; Neugebauer, J.; Nicu, V. P.; Noodleman, L.; Osinga, V. P.; Patchkovskii, S.; Philipsen, P. H. T.; Post, D.; Pye, C. C.; Ravenek, W.; Rodríguez, J. I.; Ros, P.; Schipper, P. R. T.; Schreckenbach, G.; Seldenthuis, J. S.; Seth, M.; Snijders, J. G.; Solà, M.; Swart, M.; Swerhone, D.; te Velde, G.; Vernooijs, P.; Versluis, L.; Visscher, L.; Visser, O.; Wang, F.; Wesolowski, T. A.; van Wezenbeek, E. M.; Wiesenekker, G.; Wolff, S. K.; Woo, T. K.; Yakovlev, A. L. *Amsterdam Density Functional*; SCM, Theoretical Chemistry, Vrije Universiteit: Amsterdam, The Netherlands. URL http://www.scm.com (accessed Aug 2011).

(39) Autschbach, J.; Patchkovskii, S.; Pritchard, B. *J. Chem. Theory Comput.* **2011**, *7*, 2175–2188.

(40) Dupuis, M. *Comput. Phys. Commun.* **2001**, *134*, 150–166.

(41) Govind, N.; Valiev, M.; Jensen, L.; Kowalski, K. *J. Phys. Chem. A* **2009**, *113*, 6041.

(42) Jensen, L.; Govind, N. *J. Phys. Chem. A* **2009**, *113*, 9761.

(43) Hammond, J.; Govind, N.; Kowalski, K.; Autschbach, J.; Xantheas, S. *J. Chem. Phys.* **2009**, *131*, 214103.

(44) Andzelm, J.; Rinderspacher, B.; Rawlett, A.; Dougherty, J.; Baer, R.; Govind, N. *J. Chem. Theory Comput.* **2009**, *5*, 2835.

(45) Kowalski, K.; Krishnamoorthy, S.; Villa, O.; Hammond, J.; Govind, N. *J. Chem. Phys.* **2010**, *132*, 154103.

(46) Lopata, K.; Govind, N. *J. Chem. Theory Comput.* **2011**, *7*, 1344.

(47) Iikura, H.; Tsuneda, T.; Yanai, T.; Hirao, K. *J. Chem. Phys.* **2001**, *115*, 3540–3544.

(48) Yanai, T.; Tew, D. P.; Handy, N. C. *Chem. Phys. Lett.* **2004**, *393*, 5151–57.

(49) Livshits, E.; Baer, R. *Phys. Chem. Chem. Phys.* **2007**, *9*, 2932–2941.

(50) Aquino, F.; Govind, N.; Autschbach, J. *J. Chem. Theory Comput.* **2010**, *6*, 2669–2686.

(51) Patchkovskii, S.; Ziegler, T. *J. Chem. Phys.* **1999**, *111*, 5730–5740.

(52) Malkina, O. L.; Vaara, J.; Scimmelpfennig, B.; Munzarová, M.; Malkin, V. G.; Kaupp, M. *J. Am. Chem. Soc.* **2000**, *122*, 9206–9218.

(53) Kaupp, M.; Reviakine, R.; Malkina, O. L.; Arbuznikov, A.; Schimmelpfennig, B.; Malkin, V. G. *J. Comput. Chem.* **2002**, *23*, 794–803.
(54) Neese, F. *J. Chem. Phys.* **2001**, *115*, 11080–11096.
(55) Hrobárik, P.; Malkina, O. L.; Malkin, V. G.; Kaupp, M. *Chem. Phys.* **2009**, *356*, 229–235.
(56) Komorovský, S.; Repiský, M.; Malkina, O. L.; Malkin, V. G.; Malkin, I.; Kaupp, M. *J. Chem. Phys.* **2006**, *124*, 084108–8.
(57) Repiský, M.; Komorovský, S.; Malkin, E.; Malkina, O. L.; Malkin, V. G. *Chem. Phys. Lett.* **2010**, *488*, 94–97.
(58) Neese, F. *Coord. Chem. Rev.* **2009**, *253*, 526–563.
(59) Bühl, M. NMR of transition metal compounds. In *Calculation of NMR and EPR Parameters. Theory and Applications*; Kaupp, M., Bühl, M., Malkin, V. G., Eds.; Wiley-VCH: Weinheim, Germany, 2004.
(60) Straka, M.; Kaupp, M. *Chem. Phys.* **2005**, *311*, 45–56.
(61) Bühl, M. *Annu. Rep. NMR Spectrosc.* **2008**, *64*, 77–125.
(62) Schreckenbach, G. *Int. J. Quantum Chem.* **2005**, *101*, 372–380.
(63) Schreckenbach, G.; Ziegler, T. *J. Phys. Chem. A* **1997**, *101*, 3388–3399.
(64) Jayatilaka, D. *J. Chem. Phys.* **1998**, *108*, 7587–7594.
(65) Patchkovskii, S.; Schreckenbach, G. Calculation of EPR g-tensors with density functional theory. In *Calculation of NMR and EPR Parameters. Theory and Applications*; Kaupp, M., Bühl, M., Malkin, V. G., Eds.; Wiley-VCH: Weinheim, Germany, 2004.
(66) Hrobàrik, P.; Repiskỳ, M.; Komorovskỳ, S.; Hrobàrikovà, V.; Kaupp, M. *Theor. Chem. Acc.* **2011**, *129*, 715–725.
(67) van Wüllen, C. *J. Chem. Phys.* **1998**, *109*, 392–399.
(68) Philipsen, P. H. T.; van Lenthe, E.; Snijders, J. G.; Baerends, E. J. *Phys. Rev. B* **1997**, *56*, 13556–13562.
(69) London, F. *J. Phys. Radium* **1937**, *8*, 397–409.
(70) Ditchfield, R. *Mol. Phys.* **1974**, *27*, 789–807.
(71) Fukui, H. *Magn. Res. Rev.* **1987**, *11*, 205–274.
(72) van Lenthe, E. *The ZORA Equation*, Ph.D. Thesis, Vrije Universiteit, Amsterdam, Netherlands, 1996.
(73) Bylaska, E. J.; de Jong, W. A.; Govind, N.; Kowalski, K.; Straatsma, T. P.; Valiev, M.; van Dam, J. J.; Wang, D.; Apra, E.; Windus, T. L.; Hammond, J.; Autschbach, J.; Aquino, F.; Nichols, P.; Hirata, S.; Hackler, M. T.; Zhao, Y.; Fan, P.-D.; Harrison, R. J.; Dupuis, M.; Smith, D. M. A.; Glaesemann, K.; Nieplocha, J.; Tipparaju, V.; Krishnan, M.; Vazquez-Mayagoitia, A.; Jensen, L.; Swart, M.; Wu, Q.; Van Voorhis, T.; Auer, A. A.; Nooijen, M.; Crosby, L. D.; Brown, E.; Cisneros, G.; Fann, G. I.; Fruchtl, H.; Garza, J.; Hirao, K.; Kendall, R.; Nichols, J. A.; Tsemekhman, K.; Wolinski, K.; Anchell, J.; Bernholdt, D.; Borowski, P.; Clark, T.; Clerc, D.; Dachsel, H.; Deegan, M.; Dyall, K.; Elwood, D.; Glendening, E.; Gutowski, M.; Hess, A.; Jaffe, J.; Johnson, B.; Ju, J.; Kobayashi, R.; Kutteh, R.; Lin, Z.; Littlefield, R.; Long, X.; Meng, B.; Nakajima, T.; Niu, S.; Pollack, L.; Rosing, M.; Sandrone, G.; Stave, M.; Taylor, H.; Thomas, G.; van Lenthe, J.; Wong, A.; Zhang, Z. *NWChem*, version 6.0 (2011 developer's version); Pacific Northwest National Laboratory: Richland, WA, 2011.
(74) Kendall, R. A.; Aprà, E.; Bernholdt, D. E.; Bylaska, E. J.; Dupuis, M.; Fann, G. I.; Harrison, R. J.; Ju, J.; Nichols, J. A.; Nieplocha, J.; Straatsma, T. P.; Windus, T. L.; Wong, A. T. *Comput. Phys. Commun.* **2000**, *128*, 260–283.
(75) Valiev, M.; Bylaska, E. J.; Govind, N.; Kowalski, K.; Straatsma, T. P.; Dam, H. J. J. V.; Wang, D.; Nieplocha, J.; Apra, E.; Windus, T. L.; de Jong, W. A. *Comput. Phys. Commun.* **2010**, *181*, 1477–1489.
(76) Patchkovskii, S.; Strong, R. T.; Pickard, C. J.; Un, S. *J. Chem. Phys.* **2005**, *122*, 214101–9.
(77) Vaara, J.; Ruud, K.; Vahtras, O.; Ågren, H.; Jokisaari, J. *J. Chem. Phys.* **1998**, *109*, 1212–1222.
(78) Vaara, J.; Ruud, K.; Vahtras, O. *J. Chem. Phys.* **1999**, *111*, 2900–2908.
(79) Roos, B. O.; Lindh, R.; Malmqvist, P.; Veryazov, V.; Widmark, P. *J. Phys. Chem. A* **2005**, *109*, 6575–6579.
(80) Weigend, F.; Ahlrichs, R. *Phys. Chem. Chem. Phys.* **2005**, *7*, 3295–3305.
(81) Feller, D. *J. Comput. Chem.* **2000**, *17*, 1571–1586.
(82) Schuchardt, K.; Didier, B.; Elsethagen, T.; Sun, L.; Gurumoorthi, V.; Chase, J.; Li, J.; Windus, T. *J. Chem. Inf.* **2007**, *47*, 1045–1052.
(83) Fukuda, R.; Nakatsuji, H. *J. Chem. Phys.* **2005**, *123*, 044101.
(84) Hada, M.; Wan, J.; Fukuda, R.; Nakatsuji, H. *J. Comput. Chem.* **2001**, *22*, 1502–1508.
(85) Ruiz-Morales, Y.; Schreckenbach, G.; Ziegler, T. *J. Phys. Chem. A* **1997**, *101*, 4121–4127.
(86) Kovacs, A.; Martinsen, K.; Konings, R. *J. Chem. Soc., Dalton Trans.* **1997**, 1037–1042.
(87) Preut, H.; Wilkes, B.; Naumann, D. *Acta Crystallogr.* **1990**, *C46*, 1113–1115.
(88) Ziolo, R.; Troup, J. *J. Am. Chem. Soc.* **1983**, *105*, 229–235.
(89) Ilczyszyn, M.; Lis, T.; Baran, J.; Ratajczak, H. *J. Mol. Struct.* **1992**, *265*, 293–310.
(90) Gundersen, G.; Hedberg, K. *J. Chem. Phys.* **1978**, *68*, 3548–3552.
(91) Blom, R.; Haaland, A.; Seip, R. *Acta Chem. Scand.* **1983**, *A37*, 595–599.
(92) Blake, A.; Pulham, C.; Greene, T.; Downs, A.; Haaland, A.; Verne, H.; Volden, H.; Marsden, C.; Smart, B. *J. Am. Chem. Soc.* **1994**, *116*, 6043–6044.
(93) Flaud, J.; Arcas, P.; Burger, H.; Polanz, O.; Halonen, L. *J. Mol. Spectrosc.* **1997**, *183*, 310–335.
(94) Becke, A. D. *Phys. Rev. A* **1988**, *38*, 3098–3100.
(95) Perdew, J. P. *Phys. Rev. B* **1986**, *33*, 8822–8824.
(96) Becke, A. D. *J. Chem. Phys.* **1993**, *98*, 1372–1377.
(97) Kutzelnigg, W.; Fleischer, U.; Schindler, M. The IGLO-Method: Ab Initio Calculation and Interpretation of NMR Chemical Shifts and Magnetic Susceptibilities. In *NMR Basic Principles and Progress*; Diehl, P., Fluck, E., Gunther, H., Kosfeld, R., Seelig, J., Eds.; Springer-Verlag: Heidelberg, Germany, 1990; Vol. 23.
(98) Lange, A.; Rohrdanz, M.; Herbert, J. *J. Phys. Chem. B* **2008**, *112*, 6304–6308.
(99) Belanzoni, P.; van Lenthe, E.; Baerends, E. J. *J. Chem. Phys.* **2001**, *114*, 4421–4433.
(100) Ernzerhof, M.; Scuseria, G. E. *J. Chem. Phys.* **1999**, *110*, 5029–5036.
(101) Adamo, C.; Barone, V. *J. Chem. Phys.* **1999**, *110*, 6158–6170.
(102) Manninen, P.; Lantto, P.; Vaara, J. *J. Chem. Phys.* **2003**, *119*, 2623–2637.
(103) Manninen, P.; Ruud, K.; Lantto, P.; Vaara, J. *J. Chem. Phys.* **2005**, *122*, 114107. Erratum: *J. Chem. Phys.* **2006**, *124*, 149901.
(104) Harris, R.; Mann, B. *NMR and the Periodic Table*; Academic Press: London, 1978.
(105) Jones, C.; Sharma, R.; Naumann, D. *Can. J. Chem.* **1986**, *64*, 987–990.
(106) Gombler, W. *Naturforsch.* **1981**, *36b*, 535.
(107) Naumann, D.; Herberg, S. *J. Fluorine Chem.* **1976**, *8*, 1977.
(108) Drake, J.; Khasrou, L.; Mislankar, A. *Inorg. Chem.* **1994**, *33*, 6154.
(109) Totsch, W.; Peringer, P.; Sladky, F. *J. Chem. Soc., Chem. Commun.* **1981**, 841.
(110) Jameson, C. J.; Jameson, A. *Chem. Phys. Lett.* **1987**, *135*, 254–259.
(111) McFarlane, H.; McFarlane, W. *J. Chem. Soc., Dalton Trans.* **1973**, 2416.
(112) Gedridge, R. W.; Harris, D. C.; Higa, K. T.; Nissan, R. A. *Organometallics* **1989**, *8*, 2817–2820.
(113) McFarlane, W.; Wood, R. J. *J. Chem. Soc., Dalton Trans.* **1972**, 1397.
(114) McFarlane, H.; McFarlane, W. *In Multinuclear NMR* **1987**.
(115) Jen, C. K.; Foner, S. N.; Cochran, E. L.; Bowers, V. A. *Phys. Rev.* **1958**, *112*, 1169–1182.
(116) Holmberg, R. W. *J. Chem. Phys.* **1969**, *51*, 3255–3260.
(117) Van Zee, R. J.; Ferrante, R. F.; Weltner, W., Jr. *J. Chem. Phys.* **1985**, *83*, 6181–6187.
(118) De Vore, T. C.; Weltner, W. *J. Am. Chem. Soc.* **1977**, *99*, 4700–4703.

(119) Weltner, W., Jr. *Magnetic Atom and Molecules*; Van Nostrand Reinhold: New York, 1983.
(120) Knight, L. B., Jr.; Weltner, W., Jr. *J. Chem. Phys.* **1971**, *55*, 2061–2070.
(121) Knight, L. B., Jr.; Fisher, T. A.; Wise, M. B. *J. Chem. Phys.* **1981**, *74*, 6009–6013.
(122) Hutchison, C. A., Jr.; Weinstock, B. *J. Chem. Phys.* **1960**, *32*, 56–61.
(123) Dupuis, M.; Rys, J.; King, H. *J. Chem. Phys.* **1976**, *65*, 111–116.
(124) Rys, J.; Dupuis, M.; King, H. *J. Comput. Chem.* **1983**, *4*, 154–157.